Section: Research Paper
ISSN 2063-5346

Study on synthesis, structural and luminescence properties of Eu^{3+} activated $K_2Zn_2Si_8O_{19}$ phosphor

S. D. Nimbalkar[1], D. S. Bobade[2], P. P. Bhosale[3], M. D. Shirsath[4], M. N. Rode[5].

[1] Department of Electronics, HPT Arts and RYK Science College, College Road, Nashik, India.
[2] Department of Physics, RNC Arts, JDB Commerce and NSC Science College, Nashik Road, Nashik, India.
[3] Department of Physics, New Arts, Science and Commerce College, Ahmednagar, India.
[4] Department of Physics, Dr. BAMU University, Aurangabad, India.
[5] Department of Physics, Vaidyanath College, Parali, India

***Corresponding Author Email:**
S. D. Nimbalkar: siddhunimbalkar1@gmail.com
D. S. Bobade: dsbobade1104@gmail.com

Abstract

Eu^{3+} doped potassium zinc silicate $K_2Zn_2Si_8O_{19}$ phosphors are synthesized by high temperature solid state reaction method. Eu^{3+} ions concentration dependent photoluminescence properties have been investigated and reported in this paper. The prepared powder samples are characterized by XRD and SEM measurements. The results show that the prepared samples are single phase and have irregular shape observed in morphology study. Due to different crystal field environment of Eu ion in $K_2Zn_2Si_8O_{19}$ the variation in luminescent intensity is observed. The luminescence of Eu^{2+} ion consists of the $4f^6 5d_1 \rightarrow 4f^7$ ($^8S_{7/2}$) broad-band emission. Along with this, emission bands at 594 and 615 nm are attributed to the $^5D_0 \rightarrow {}^7F_j$ (J=1, 2) transitions of Eu^{3+} ion are also obtained. PL emission showed the emissions at 594 nm and 615 nm which denotes the lamp application.

Keywords: phosphor; photoluminescence; aluminosilicates; solid state reaction method;

1. Introduction

Luminescent nano-materials represent a cutting-edge field in science, presenting exciting challenges for fundamental research and revolutionary advancements in multiple areas, including electronics, photonics, nanotechnology, displays, lasers, detection, optical amplification, fluorescent sensing, biomedical engineering, and environmental control. The study of inorganic luminescent materials has been extensively conducted, particularly for their application in display materials. These materials are currently widely employed in high-definition televisions (HDTVs), plasma display panels (PDPs), cathode ray tubes (CRTs), and field emission displays (FEDs) [1-6].

The development of inorganic rare earth doped luminescent materials with high absorption ranging from near ultraviolet to the blue region has garnered continuous interest. While nitride phosphors exhibit promise, their preparation necessitates stringent conditions such as high temperature and nitrogen pressure. On the other hand, sulfide phosphors [7] suffer from chemical instability and insufficient lifespan. Alternative host materials, including aluminates, borates, and silicates [8], have emerged as other promising candidates for light emitting diodes (LEDs), particularly for white LED applications. In recent times, nitride phosphors have gained attractiveness among researchers due to their exceptional characteristics and are gradually replacing sulfides and orthosilicates in solid-state lighting [9].

Eu^{3+} ion-activated phosphors are well-known for their broad-band emission, which arises from transitions between the $^4f_7$ ground state and the $^4f_6$ 5d excited state. The luminescence of Eu^{2+} is heavily influenced by the surrounding host structure and crystallographic distortions due to the sensitivity of the 5d electrons of Eu^{2+}. Extensive attention has been given to Eu^{3+}-activated silicate-based long afterglow materials due to their notable chemical and physical stability. However, their long afterglow property is comparatively inferior to that of aluminium-based long afterglow phosphors (e.g., $SrAl_2O_4$: Eu, Dy [10]). Eu^{3+} doped $Ba_2Zn_3Si_3O_{11}$ displays characteristic two-peak emission spectra with one weak emission band at 440 nm and another stronger one at 540 nm. The emission intensity has the dependence on Eu^{2+} doping [9]. Extensive studies have been conducted on Eu^{2+}-doped phosphors such as $Zn_4Al_{22}O_{37}$: Eu [13] and Sr_2SiO_4: Eu [14].

This study focuses on the synthesis of potassium zinc silicate phosphors, specifically $K_2Zn_2Si_8O_{19}$: Eu using the high-temperature solid-state reaction method. The concentration of europium ions was taken as 0.1, 0.2, 0.5 and 1 mole%. The photoluminescence properties of the phosphors were investigated as a function of the Eu ion concentration.

2. Experimental Details

Europium-doped $K_2Zn_2Si_8O_{19}$ phosphors were prepared through a solid-state reaction method at high temperature, utilizing high-purity (AR grade) KNO_3, ZnO, SiO_2.H2O, and Eu_2O_3 as starting materials. The stoichiometric ratios of all precursors were thoroughly ground in a mortar and pestle for one hour. The resulting mixtures were heated at 800°C for 24 hours and then slowly cooled to room temperature. The obtained samples were further ground for an additional hour until they reached a fine powder form. The synthesized powder samples were characterized for their phase purity and crystallinity using X-ray powder diffraction (XRD).

These synthesized samples were further utilized for doping Eu ions at various concentrations. The resulting products were analyzed using XRD, a scanning electron microscope (SEM, LEO-1530FE) equipped with energy-dispersive X-ray spectroscopy (EDS) (EDAX, DX-4). Infrared measurements were conducted using a Shimadzu IR spectrophotometer, and UV-Vis absorption spectra were recorded on a Shimadzu recording spectrometer. Photoluminescence measurements, including excitation and emission spectra, were recorded on a Shimadzu RF5301PC spectrofluorophotometer with a slit width of 1.5 nm for each measurement.

3. Results and Discussion

3.1 X-ray diffraction analysis:

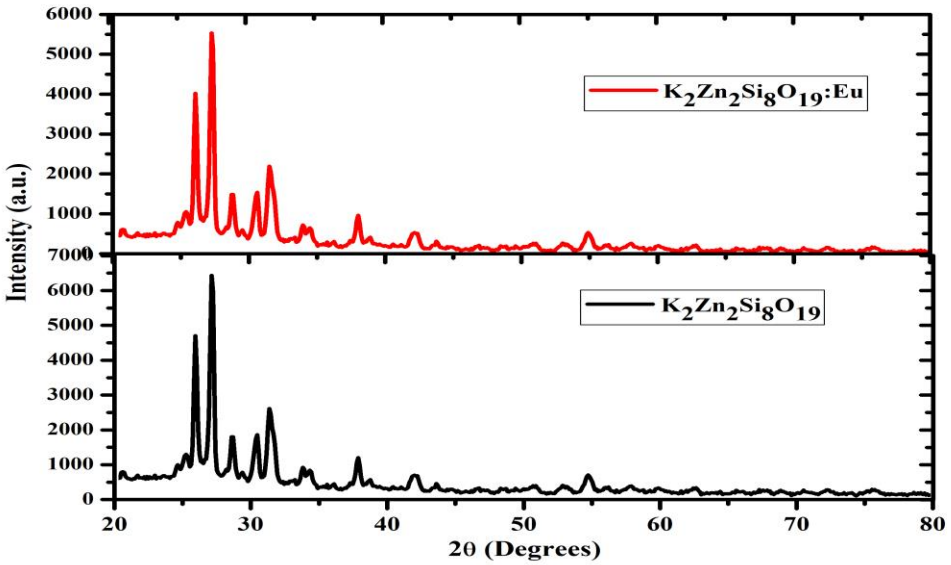

Figure 1: XRD powder diffracion paern of $K_2Zn_2Si_8O_{19}$:Eu

Figure 1 presents the X-ray diffraction (XRD) pattern of the host $K_2Zn_2Si_8O_{19}$ and Eu-doped $K_2Zn_2Si_8O_{19}$ phosphor synthesized at 900°C. The majority of the observed peaks can be assigned to the $K_2Zn_2Si_8O_{19}$ phase. This suggests that the introduction of Eu^{3+} dopants does not give rise to new phases during the reaction process. The limited concentration of Eu^{3+} ions in the host compounds contributes to this outcome. It indicates that a solid-state solution is formed in all the samples. Our findings are consistent with previous reports [15].

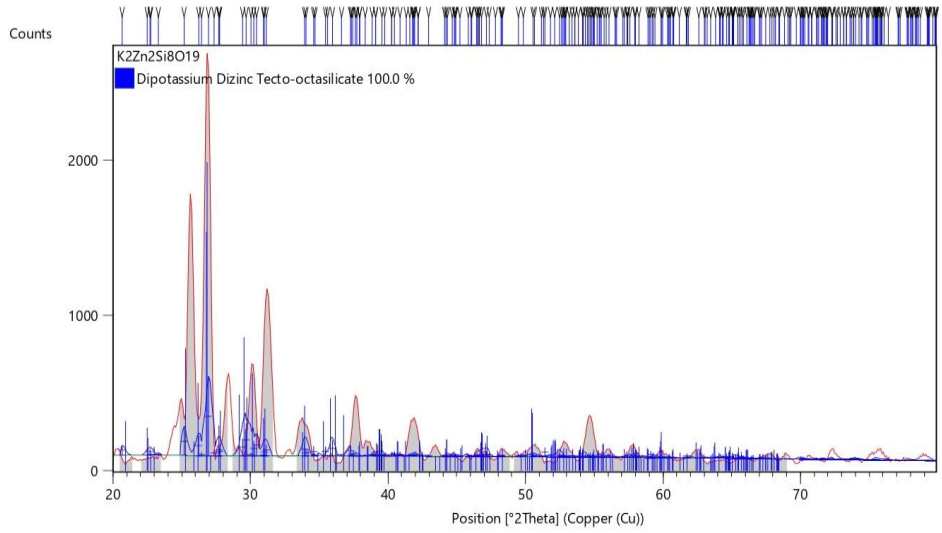

Figure 2: Matched pattern of $K_2Zn_2Si_8O_{19}$

The peak positions of $K_2Zn_2Si_8O_{19}$ and $K_2Zn_2Si_8O_{19}$: Eu matched well with the standard pattern ICSD file no. 98-002-6261 as shown in **Figure 2**. The crystal structure of $K_2Zn_2Si_8O_{19}$ and $K_2Zn_2Si_8O_{19}$: Eu was determined to be monoclinic based on the XRD analysis. It was confirmed that the synthesized samples consisted of a single phase. Additionally, the coordination of K, Zn, Si, and O atoms was verified using infrared spectroscopy.

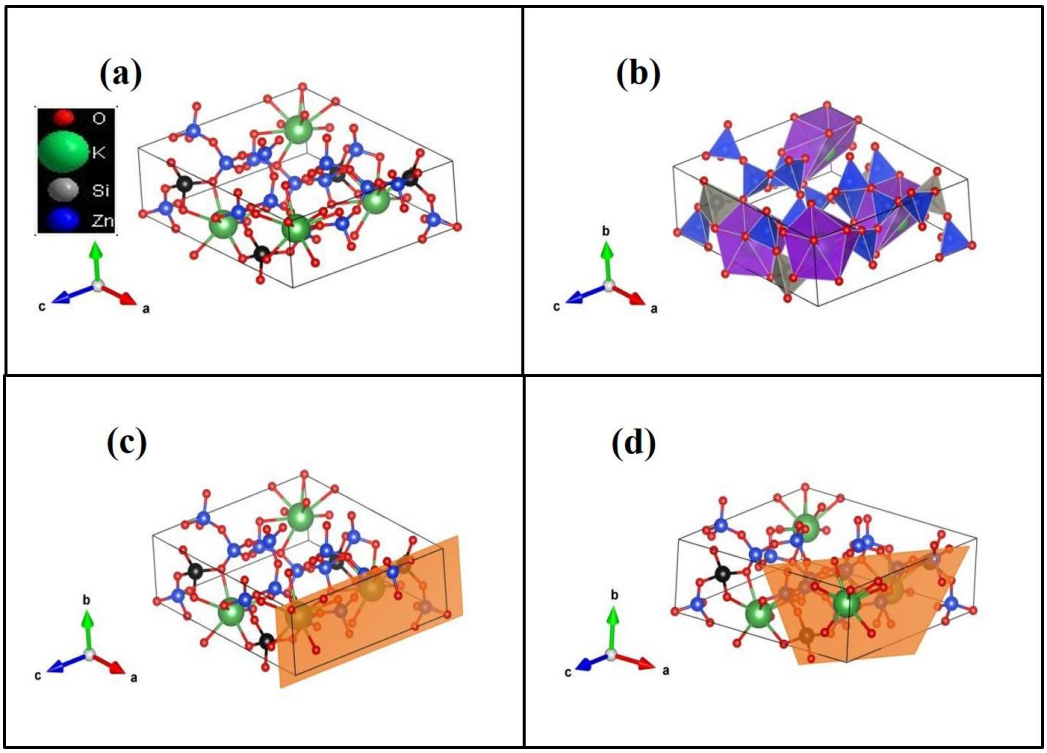

Figure 3: (a) Co-ordination ball and stick model (b) Polyhedral model (c) [110] lattice plane and [513] lattice plane of the $K_2Zn_2Si_8O_{19}$

The co-ordination ball and stick model of the $K_2Zn_2Si_8O_{19}$ is shown in **Figure 3(a)**. In this diagram we can see that the oxygen atoms are coordinated to the Zn, Si and K atoms. These atoms have occupied the central position of the polyhedral geometry as denoted in figure 3(b). The lattice plane having Miller indices [110] and [513] are shown in figure 3(c) and 3(d).

3.2 SEM and EDS Analysis:

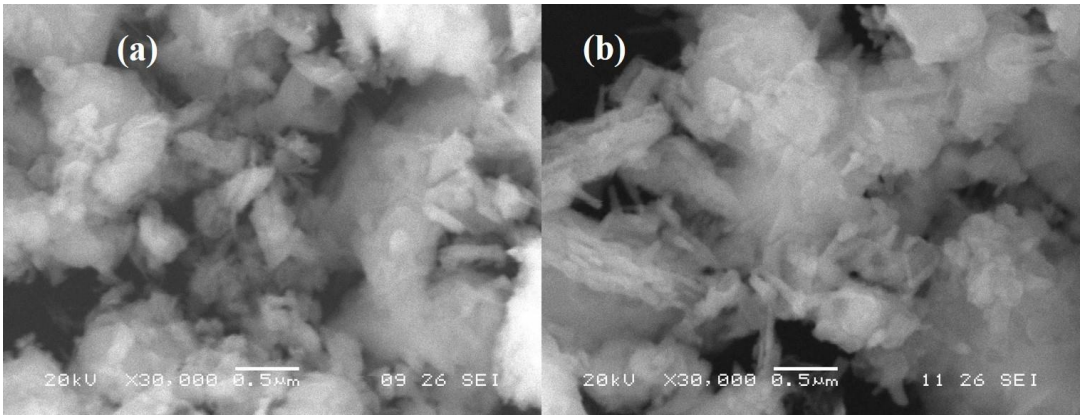

Figure 4: SEM images of (a) $K_2Zn_2Si_8O_{19}$ host and $K_2Zn_2Si_8O_{19}$: Eu

Figure 4 illustrates the scanning electron microscopy (SEM) images of $K_2Zn_2Si_8O_{19}$ and $K_2Zn_2Si_8O_{19}$: Eu. The images reveal that the grains exhibit irregular shapes. The particle morphology indicates the presence of highly agglomerated crystallites, and the average size of the crystals falls within the sub-micrometer range. The estimated grain sizes of the synthesized samples range from less than 0.5 µm to 3 µm.

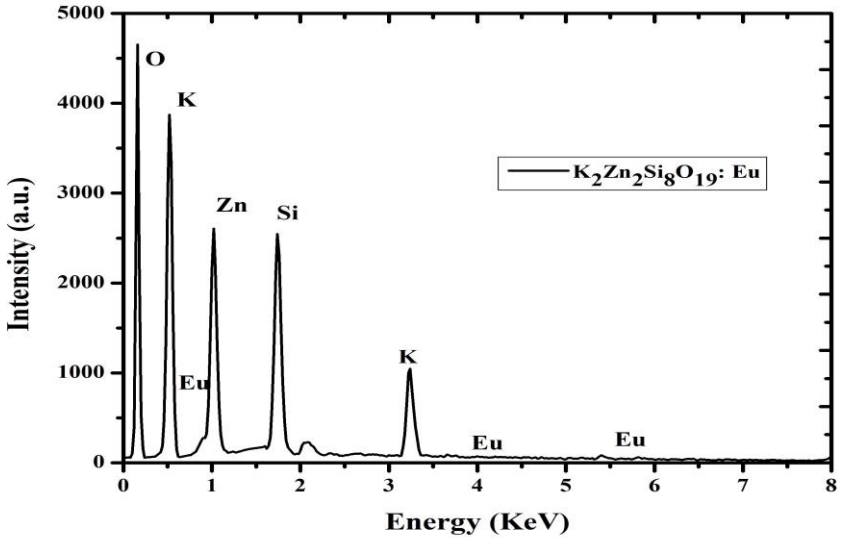

Figure 5: Energy dispersive spectrum of $K_2Zn_2Si_8O_{19}$: Eu

Table 1: Elemental composition of $K_2Zn_2Si_8O_{19}$

Elements	$K_2Zn_2Si_8O_{19}$		$K_2Zn_2Si_8O_{19}$:Eu	
	Weight %	Atomic %	Weight %	Atomic %
O	60.25	61.40	60.32	61.31
Si	25.10	25.70	25.20	25.78
Zn	7.01	6.35	6.98	6.34

K	7.64	6.55	6.96	6.51
Eu	0	0	0.10	0.06

Table 1 presents the relative elemental composition of Eu-doped $K_2Zn_2Si_8O_{19}$ in which the presence of K, Zn, Si, and O and concentrations are shown. The doping concentrations for each sample are also provided. The results reveal that the europium concentration in the prepared samples is relatively low. Additionally, we have included the EDS graph as shown in **Figure 5** of the prepared 8 mole% Eu-doped $K_2Zn_2Si_8O_{19}$ sample for reference.

3.3 Infrared Spectroscopy Analysis:

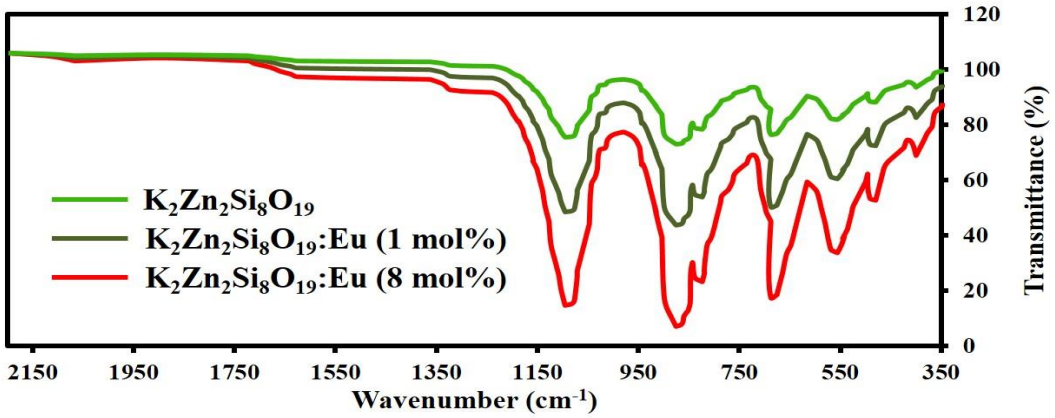

Figure 6 : Infra-red spectra of $K_2Zn_2Si_8O_{19}$ and $K_2Zn_2Si_8O_{19}$ Eu

Figure 6 depicts the FTIR spectra which exhibiting absorption bands at 1040, 860, 620, 560 and 4080 cm^{-1} for $K_2Zn_2Si_8O_{19}$ and $K_2Zn_2Si_8O_{19}$: Eu. The IR spectrum of $K_2Zn_2Si_8O_{19}$ and $K_2Zn_2Si_8O_{19}$: Eu clearly shows the strong absorption band due to Si–O vibrations at 1040 cm^{-1} for $K_2Zn_2Si_8O_{19}$ hosts in the mid-infrared region, whereas, vibrations of Zn–O are seen at 560 cm^{-1} and 408 cm^{-1}. Absorption bands near 860 and 620 cm^{-1} are due to K– O respectively [16, 17].

3.4 UV-visible spectroscopy analysis:

In order to examine the optical properties of Eu-doped $K_2Zn_2Si_8O_{19}$ and $K_2Zn_2Si_8O_{19}$: Eu phosphors, we initially analyzed the absorption spectra of the prepared samples. Figure 3 displays the absorption spectra of 8 mol% Eu-doped $K_2Zn_2Si_8O_{19}$ and $K_2Zn_2Si_8O_{19}$ host. The absorption spectra presented in **Figure 7** specifically correspond to 8 mol% doping concentration in $K_2Zn_2Si_8O_{19}$: Eu phosphors.

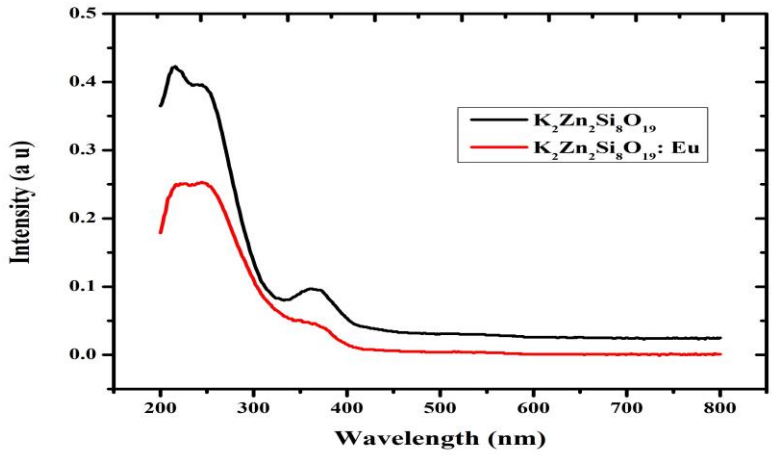

Figure 7: UV-visible Absorption spectra of $K_2Zn_2Si_8O_{19}$ and $K_2Zn_2Si_8O_{19}$: Eu

The UV-Visible spectra reveal that Eu^{2+} doped $K_2Zn_2Si_8O_{19}$ phosphors exhibit a decrease in intensity compared to the host spectra. Additionally, the absorption spectra show a blue shift in the presence of Eu doping, indicating a reduction in the band gap of the host material due to the incorporation of Eu ions.

The calculated band gap energies based on the absorption spectra are as follows: for $K_2Zn_2Si_8O_{19}$, it is 3.63 eV. In the case of Eu-doped samples, the band gap energies are 3.42 eV. These results indicate that the band gap of the phosphors decreases due to Eu doping.

3.5 Photoluminescence properties of $K_2Zn_2Si_8O_{19}$: Eu

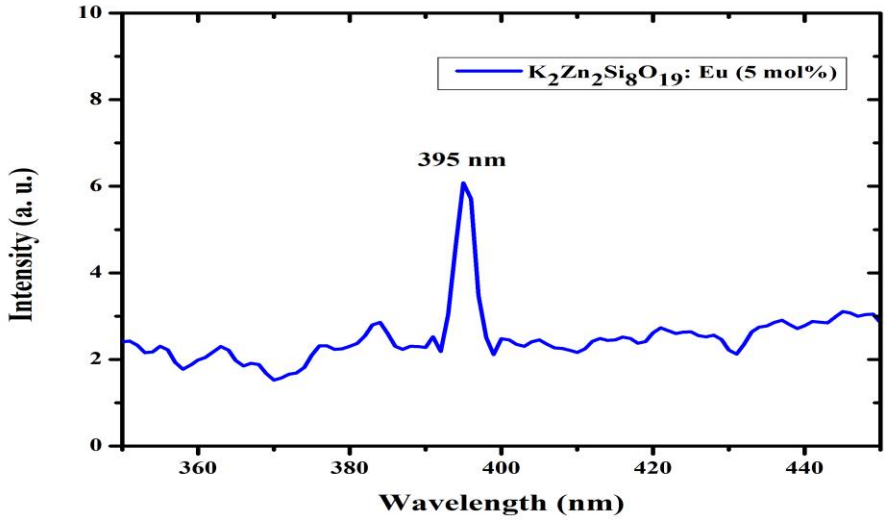

Figure 8: Excitation spectrum of $K_2Zn_2Si_8O_{19}$: Eu (1 mol%) monitored at 615 nm

The excitation spectrum of Eu doped $K_2Zn_2Si_8O_{19}$ phosphor under an emission wavelength of 615 nm is shown in the inset of **Figure 8**. The maximum excitation wavelength value is selected to obtain the emission spectrum of Eu doped $K_2Zn_2Si_8O_{19}$.

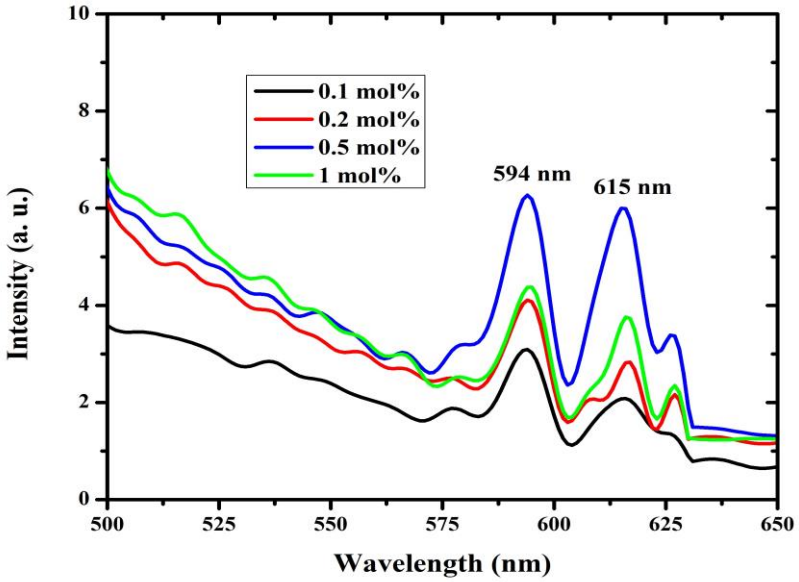

Figure 9: Emission spectra of $K_2Zn_2Si_8O_{19}$: Eu monitored at 395 nm excitation.

The emission spectrum of Eu doped $K_2Zn_2Si_8O_{19}$ phosphor under an emission wavelength of 615 nm is shown in the inset of **Figure 9**. Within the range of 420 nm to 500 nm, the spectra exhibit a broad emission peak with a slight doublet nature, likely attributed to two types of lattice sites occupied by Eu^{3+} in the $K_2Zn_2Si_8O_{19}$: Eu host. The dominant peak is observed at 430 nm ($^5D_3 \rightarrow {}^7F_1$), followed by an emission around 445 nm, and attributed to the $^4f_6{}^5d_1 \rightarrow {}^4f_7$ ($^8S_{7/2}$) transitions of Eu^{3+} ions. Additionally, in Figure 5, narrow bands are observed in the range of 500 nm to 625 nm, with the 615 nm band exhibiting the maximum intensity. These peaks mainly arise from the $^5D_1 \rightarrow {}^7F_1$ (540 nm), $^5D_0 \rightarrow {}^7F_1$ (594 nm), $^5D_0 \rightarrow {}^7F_2$ (615 nm), and $^5D_0 \rightarrow {}^7F_3$ (650 nm) transitions of Eu^{3+} ions, explaining the yellow, orange, and red emission in the visible spectra.

Color representation in lighting calculations is based on the 1931 CIE chromatic color coordinates, which recognize the three primary colors of the human visual system: red, green, and blue [22, 23]. The color of any light source can be represented on the (x, y) coordinate in this color space. Color purity was compared to the 1931 CIE Standard Source C (illuminant Cs with coordinates of (0.3101, 0.3162)). The chromatic coordinates (x, y) were calculated using the radiant imaging color calculator program [24]. The color coordinates of the Eu doped $K_2Zn_2Si_8O_{19}$ phosphors, representing red ($x \approx 0.653$, $y \approx 0.331$), orange ($x \approx 0.591$, $y \approx 0.410$), green ($x \approx 0.227$, $y \approx 0.752$), and blue ($x \approx 0.158$, $y \approx 0.017$), are shown in Figure 7 as solid circle signs (•). The location of these color coordinates on the CIE chromaticity diagram,

presented in Figure 8, indicates that the color properties of the phosphor powder prepared by solid-state reaction approach those required for field emission displays.

The dominant wavelength refers to the single monochromatic wavelength that appears to have the same color as the light source. It can be determined by drawing a straight line from one of the CIE white illuminants (Cs with coordinates of (0.3101, 0.3162)) through the measured (x, y) coordinates until the line intersects the outer locus of points along the spectral edge of the 1931 CIE chromatic diagram.

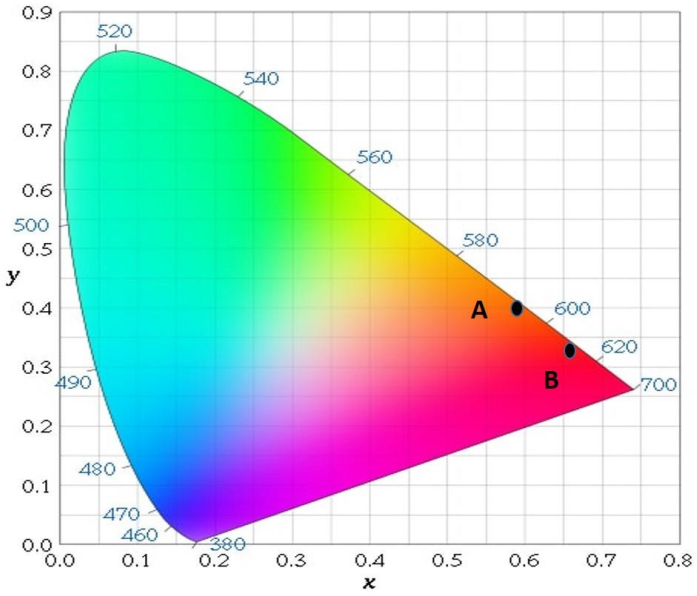

Fig. 8 : CIE chromatic diagram showing the chromatic coordinates.

4. Conclusions

Eu^{3+}-doped $K_2Zn_2Si_8O_{19}$ phosphors were synthesized using the high-temperature solid-state diffusion method. The XRD analysis confirmed the crystal structure of the prepared phosphors. SEM provided information about the grain size, revealing that the phosphors had grains of several micrometers in size. PL measurements revealed that the Eu^{3+} ions acted as luminescent centers in $K_2Zn_2Si_8O_{19}$ and exhibited characteristic emissions under excitation at 395 nm. The emissions were observed at wavelengths of 420 nm, 445 nm, 580 nm, 595 nm, and 615 nm with high intensity. Eu^{3+}-doped $K_2Zn_2Si_8O_{19}$phosphor exhibited a dominant broad emission peak in the blue region and a prominent emission at 615 nm (red), making it a more suitable material applicable in lamps.

References

[1] C.M. Mehare, Y.R. Parauha, N.S. Dhoble, C. Ghanty, S.J. Dhoble, J. Mol. Struct. 2020, 1212, 127957.

[2] Q. He, C. Hu, Opt. Mater. 2014, 38, 286.
[3] Y.R. Parauha, V. Chopra, S.J. Dhoble, Mater. Res. Bull. 2020, 131, 110971.
[4] P. Wang, X. Xu, J.Qiu, X. Yu, Q. Wang, Opt. Mater. 2014, 36, 1826.
[5] C. R. García, L. A. Diaz-Torres, J. Oliva, G. A. Hirata, Opt. Mater. 2014, 37, 520.
[6] S. Li, X. Peng, X. Liu, Z. Huang, , Opt. Mater. 2014, 38, 242.
[7] TENG Xiaoming, ZHUANG Weidong, HU Yunshe, HUANG Xiaowei , J.Rare Earths,26(5), (2008) 652.
[8] S.K. Raut, N.S. Dhoble, K. Park, S.J. Dhoble, Materials Chem. and Phys. 147 (2014) 594.
[9] Hung Quang Trinh, Jin Oh Jo, Sang Baek Lee, Young Sun Mok, Current Appl.Phys. 14 (2014) 1051.
[10] A. Diaz, D.A. Keszler, Mater. Res. Bull. 31 (1996) 147.
[11] Abha H. Oza, N.S. Dhoble, S.J. Dhoble, Nucl. Inst. and Methods in Phys. Resea. B 344 (2015) 96.
[12] F. Clabau, A. Garcia, P. Bonville, D. Gonbeau, T. Le Mercier, P. Deniard and S. Jobic, J. Solid State Chem., 181(2008)1456.
[13] Bobade, Dinesh S., Yatish R. Parauha, Sanjay J. Dhoble, and Prabhakar B. Undre. "Study on luminescence properties of Ce^{3+} and Eu^{3+} ions in a nanocrystalline hexagonal $Zn_4Al_{22}O_{37}$ novel system." *Luminescence* 37(3), 500-513 (2022).
[14] Bobade, D. S., and P. B. Undre. "Synthesis and Luminescence Properties of Eu^{3+} Doped Sr_2SiO_4 Phosphor." Integrated Ferroelectrics 205(1), 72-80 (2020).
[15] Joachim Deubener, Martin Sternitzke, Gerd Muller, American Mineralogist, 76 (1991) 1620.
[16] Ashok V. Borhade, Arun G. Dholi, Sanjay G. Wakchaure, Dipak R. Tope, Desalination and Water Treatment 50 (2012) 157.
[17] Ashwini Kumar, S.J. Dhoble, D.R. Peshwe, Jatin Bhatt, J. Alloys and Comp. 578 (2013) 389.
[18] S. Rani, S. Sanghi, A. Agarwal, V.P. Seth, Spectrochimica Acta Part A 74 (2009) 673.
[19] Martinus H.V. Werts, Y. Ronald, T.F. Jukes, Jan W. Verhoeven, Phys. Chem. Chem. Phys. 4 (2002) 1542.
[20] Baochang Cheng, Shengchun Qu, Huiying Zhou, Zhanguo Wang, Nanotechnology 17 (2006) 2982.
[21] Fuping Du, Yosuke Nakai, Taiju Tsuboi, Yanlin Huang, Hyo Jin Seo, J. Mater. Chem. 21 (2011) 4669.
[22] G.B. Stringfellow, M.G. Craford (ed.), vol. 48, ed. by R.K.Willardson, E.R.Weber, Academic Press, San Diego, 1997.
[23] S. Shionoya, W.M. Yen, *Phosphor Handbook* (Phosphor Research Society, CRC Press, Boca Raton, 1998), p. 459.

[24] Color Calculator version 2, A software from Radiant Imaging, Inc., 2007